Stress waves in composite materials

B. E. Clements, J. N. Johnson, and R. S. Hixson
Los Alamos National Laboratory, Los Alamos, New Mexico 87545
(Received 5 June 1996)

The method of cells (MOC) developed by Aboudi provides a powerful means for studying the propagation of waves through systems having complicated internal cell structure [Wave Motion **9**, 141 (1987)]. Laminated materials are a common example. The method can handle harmonic waves and also *transient* waves arising from a finite duration impulse. The method is sufficiently robust to treat impact, as we show here. Both linear and nonlinear elastic-stress-strain relations can be included. The present work generalizes the method to include viscoelastic materials (such as polymers), systems with cell structure deviating from perfect periodicity (including random), and systems simulating actual impact experiments. We test the theory by comparing our results with measurements taken from a flat-plate impact experiment. The system investigated was a bilaminate composed of unit cells of epoxy and epoxy-graphite subcells. Using known and estimated material parameters, we find that the MOC gives a reasonable representation of the data. We then address some features of the experimental data that have not yet been explained by other theoretical methods. The importance of unit cell periodicity is tested by adding a random incremental width to each unit cell. Finally, the shortcomings of the MOC caused by using a truncated series expansion for the particle displacements, and neglecting plastic flow and nonadiabatic effects are discussed. [S1063-651X(96)10712-1]

PACS number(s): 03.40.Dz, 03.40.Kf, 62.30.+d, 62.50.+p

I. INTRODUCTION

Laminated media serve as mechanical wave filters in the same way as a lattice of point particles connected by mechanical springs. The added complication is that wave propagation can also take place *within* each component. In this sense mechanical energy propagation in one-dimensional laminates is more analogous to the wave mechanics of electrons in solids when described in terms of the Kronig-Penney model; in fact the dispersion relations for the two cases are essentially identical [1]. The standard treatment of wave propagation in mechanical systems involves the investigation of material response to sinusoidal disturbances of infinite extent. That is, we simply obtain the dispersion relation which gives the relationship between the wave number k and the angular frequency ω (or equivalently, between the phase velocity $c=\omega/k$ and the wave number). Transient wave propagation (for example, waves of finite duration) can be treated in these materials by a Fourier decomposition of the boundary condition, allowing each Fourier component to propagate with its appropriate phase velocity, and then reconstructing the pulse at some point removed from the input boundary [2]. In fact, in certain mechanically dispersive systems the dispersion relation is itself obtained by the Fourier transform method [3]. These results, of course, apply only to linearly elastic materials, although with considerable effort they may be made to apply to linear viscoelastic solids. Also, in the case of laminated materials, perfect periodicity is required.

The application to nonlinear elastic materials and laminates with imperfectly positioned components (either accidentally or by design) require other methods of solution. A particularly powerful method of treating the nonlinear, inelastic deformation of composite materials in three spatial dimensions is the method of cells (MOC) attributed to Aboudi [4,5]. MOC gives excellent agreement with exact results for dispersion relations obtained by invoking the Floquet theory, for example, in the case of harmonic waves propagating through a linear elastic periodic system [6], as it does when compared to exact ray theory [7] for transient wave propagation. While this method is familiar in engineering applications, it is less known in physics research. Consequently, one goal of this paper is to demonstrate its wide versatility, including many potential applications in physics.

Generally, the MOC is designed for systems that are made up of a periodic repeating assembly of unit cells. The unit cells are further divided into subcells; the unit cells and subcells will be labeled by p and α, respectively. Here we consider planar laminates normal to the x direction. The displacement is uniaxial and in the x direction. The continuous local spatial variable within subcell α is denoted by $\overline{x}$. The MOC method involves expanding the particle displacement within each subcell of a composite material in terms of Legendre polynomials. Of course, any complete set of basis functions will do, but these appear to be the most useful. For example, we write this expansion in one spatial dimension (which is the case of interest here) as

$$u^{\alpha,p}(\overline{x},t)=\sum_{l=0}^{\mathcal{N}} \mathcal{U}_l^{\alpha,p}(t)P_l(2\overline{x}/d_\alpha). \tag{1.1}$$

All the time dependence in the displacement is now contained in the *cell coefficients*, $\mathcal{U}_l^{\alpha,p}(t)$. The essence of the MOC approach is to substitute Eq. (1.1) into the equation of motion

$$\frac{\partial \sigma^{(\alpha,p)}(\overline{x},t)}{\partial \overline{x}}=\rho_{\alpha,p}\ddot{u}^{(\alpha,p)}(\overline{x},t), \tag{1.2}$$

and integrate the result over a unit cell. Upon doing so the stress, $\sigma^{(\alpha,p)}$, evaluated at the cell boundaries emerges as an

explicit variable in the equations. These are then removed from the equations by imposing stress (and also displacement) continuity at all internal cell boundaries separating materials of different mass densities $\rho_{\alpha,p}$. The stresses at the external cells are forced to match the desired applied boundary conditions. A more detailed discussion of the MOC is deferred to Sec. II A.

The MOC has been applied to composites using linear elasticity theory, and to a slightly lesser degree to systems where nonlinear elasticity is important. We find in the present work that nonlinear elastic contributions are very important and must be kept. By a simple extension of the Aboudi theory we have also generalized the MOC to handle (approximately) viscoelastic materials. The formalism is based on *the standard viscoelastic-solid model* [8], and is developed in Sec. II B. This extension allows one or more of the components of the composite to have stress-relaxation properties. While we test the theory using several common polymeric compounds such as epoxy and PMMA (polymethylmethacrylate), there is no reason, *a priori*, that the viscoelastic properties of other more viscous and perhaps *exotic* materials (including those of biological relevance such as those found in lipid bilayers [9]) could not be investigated by this technique.

Our second contribution is to adapt the MOC to model the conditions found in actual impact experiments. A standard technique for achieving large uniaxial stresses in a sample is to use some controlled means for firing a flat projectile, a so-called flyer plate, at the target material and then studying material response in one spatial dimension. To allow for this scenario requires two changes in the formalism. First, the combined flyer plate and composite become the new system; stress waves initiated by the impact must be allowed to travel in both materials, including being transmitted and reflected at the flyer-composite interface. Second, appropriate initial and boundary conditions must be constructed in terms of the known quantities — the flyer velocity and material parameters. The first of these requires no true alterations in the MOC formalism, but only changes in the detailed numerics. The homogeneous flyer is zoned into ''fictitious'' unit cells, and stress and displacement continuity are forced at each cell interface, similar to what is done in the composite. Our arguments for determining the appropriate boundary conditions to match the impact experiment are stated in Sec. II E, and again they rely on using stress and displacement continuity, but this time at the impact interface. The crucial step is to relate the flyer velocity to the particle speed U_p, which can then be related through mass and momentum conservation [10] to the stress (and shock speed U_s) since $\sigma=\rho U_s U_p$; ρ is the average mass density.

Having made these generalizations we are then able to compare MOC results to high-velocity shock data that are taken from an impact experiment performed on a periodic laminate of epoxy and epoxy graphite. In this experiment a flyer plate traveling at 0.5003 km/s impacted with the laminated target. Since the stress reached a value of 17 kbar (and a volume strain of approximately 10%) this experiment provides a rather stringent test on the theory — it also provides the reader with a means of assessing the reliability of the MOC in an actual impact situation. A discussion of the comparison is given in Sec. III C.

Previous work by Aboudi [11] investigated the MOC in comparison with other calculations of transient wave propagation; particularly ray theory (or characteristic theory) in linear elastic materials. The important difference here is that we are making a comparison of the MOC with experimental data. This is an important test of the analytic technique because it brings into consideration our imperfect knowledge of material properties. At very low impact stresses, linear elastic effects are well represented by second-order, adiabatic elastic moduli. In viscoelastic solids there is always the complication of dissipation at finite strain rates. At higher impact stress, nonlinear elasticity and plastic flow can occur. The net effect of comparing the MOC with experimental data is that we can see its strengths and weaknesses in actual applied situations. The need for good experimental information on each component becomes an explicit part of the assessment of the method.

Our next step was to evaluate the role of the nonideal periodicity of the unit cell structure in the composite. This was done by adding a small but randomly chosen additional width to a minimum allowed value for each cell. A small amount of disorder was found to have little, but still observable, influence on the results (Sec. III E). This is an important observation since cell periodicity in the experiment was not perfect, as in most real applications. We also point out that one should be able to use the MOC to probe wave propagation in systems characterized as having significant disorder. One can then use the MOC to study fundamental issues such as acoustic localization in random layered materials. Although illuminating theoretical work has already been devoted to this problem [12,13], much of it applies to model systems. The MOC, on the other hand, is designed to handle true physical systems where material parameters play a crucial role. This and related problems remain an active area of experimental research [14].

An obvious question to ask is why not solve for wave propagation in the one-dimensional system using finite-difference methods [15]. This would give as much accuracy as desired and could certainly handle all types of material behavior (nonlinear elastic, viscoelasticity, viscoplasticity, and so on) [16]. Indeed many of these material properties are known to be of great importance when high stress fields are present although they are also difficult to incorporate into the MOC approach [17,18]. (Note, in Sec. IV a summary of the shortcomings of the MOC will be addressed.) It is true that we could solve for impact of a one-dimensional composite system by finite difference, but there are several reasons why we choose to pursue methods like the MOC.

First, we are not looking for a precise numerical solution to a particular problem in heterogeneous material behavior, but rather a method that will lead to approximate (but still reliable) representations of transient wave motion at finite wavelengths in layered materials. From a computational point of view, the MOC method is considerably less computationally intensive compared to a finite-difference calculation on the same system. A finite-difference approach is challenged by the fact that material interfaces with large acoustic impedance mismatches will require a very fine zoning of the spatial grid. While grid zoning is not a negligible consider-

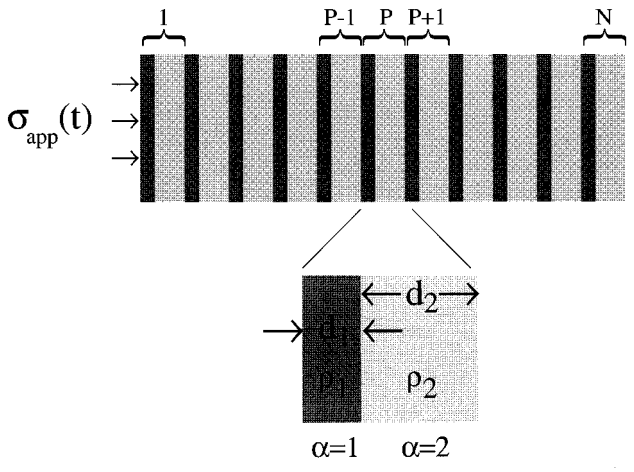

FIG. 1. Schematic of a laminated system to which the MOC is typically applied. Unit cells, labeled 1 through N are subjected to an external stress $\sigma_{app}(t)$. Each unit cell contains two subcells ($\alpha=1,2$) with subcell widths d_1 and d_2 and mass densities ρ_1 and ρ_2.

ation in the MOC, it seems to be less severe and thus the MOC remains tractable even in three-dimensional composites.

Second, the MOC offers an obvious scheme for making approximations. To suit the problem at hand one can truncate the MOC expansion (1.1) at the appropriate value of $\mathcal{N}$. For some applications it is sufficient to replace the discrete cell structure of the composite with a homogeneous continuum that possesses the same mechanical and dispersive properties in an average sense. As an example, the quasistatic, first-order theory [expansion of u in Eq. (1.1) out to $\mathcal{N}=1$] is very good for a long-wavelength response of laminates, but gives only the average moduli of the composite and none of the dispersive properties [19]. In these applications the entire unit cell p is thought of as being mapped into a single point in coordinate space. This is the case when one calculates the long-wavelength limit of dispersion relations for a laminated material; the discrete laminate can be replaced by a continuum model. In other applications, such as those presented here, we retain the time dependence in the displacements, the acceleration terms, and the full discrete nature of the lamination. This is done in an attempt to get reasonable dispersion effects. For that purpose truncating the expansion at $\mathcal{N}=2$ is probably sufficient.

II. GENERALIZED SECOND-ORDER ABOUDI THEORY

In this section we review Aboudi's dynamical second-order theory of the method of cells. We shall restrict our discussion to the special case of longitudinal waves propagating normal to the layering in one-dimensional laminates. In spite of the restriction to one dimension, this situation can be realized in conventional planar impact-plate experiments in which target samples in lateral directions are sufficiently large. Under these conditions, release waves originating from the lateral surfaces do not affect the direct longitudinal waves through the duration of the experiment. Also, although we are explicitly considering longitudinal waves, formally the theory applies (with a change of modulus) to shear deformation as well.

In the initial application of this method [11,20], the Aboudi formalism initiates a stress wave in these systems by applying a time dependent stress $\sigma_{app}(t)$ to one side of the composite system. Transient waves are then studied as they pass various locations within the composite. In the one-dimensional applications, the composite is comprised of periodic repeating unit cells; each of these consists of two component subcells forming the laminate. The setup is shown in Fig. 1. The thickness and mass density of each constituent is denoted by d_α and ρ_α, respectively. The total width of a unit cell is then d_1+d_2. In these studies, $\sigma_{app}(t)$ is taken to be a smooth, albeit rapidly increasing, analytic function of time. For this situation the Aboudi formalism has been reviewed in detail [4,19,21,11,20] and it suffices here to give only a brief overview before proceeding directly to our extensions of the formalism as they apply to the systems of interest in the present work. These extensions are the following: (i), to include viscoelastic effects; (ii), to introduce a shock into the system by allowing a flyer plate to impact with the composite sample; and (iii), to allow for arbitrary system geometries by removing restrictions that the system has perfect cell periodicity.

A. Overview of the Aboudi formalism

At the heart of the MOC method is the assumption that the particle displacement u can be represented by a low-order truncation of a Legendre series of Eq. (1.1). Letting $\overline{x}$ represent a local position variable measured relative to the center of subcell α of unit cell p, the displacement to second order in the Legendre series can be cast into the form

$$u^{(\alpha,p)}(\overline{x},t)=w^{(\alpha,p)}(t)+\overline{x}\phi^{(\alpha,p)}(t)+\frac{1}{2}\left[3\overline{x}^2-\frac{d_{\alpha,p}^2}{4}\right]U^{(\alpha,p)}(t). \quad (2.1)$$

(Here, we already anticipate looking at systems with broken periodicity and have attached the additional unit cell label to d.) The time-dependent cell coefficients $w^{(\alpha,p)}(t),\phi^{(\alpha,p)}(t)$ and $U^{(\alpha,p)}(t)$, are determined by a solution of the equations of motion [Eq. (1.2)] combined with stress and displacement continuity at subcell interfaces.

The first step in the procedure is to substitute the displacement, Eq. (2.1), into the equation of motion Eq. (1.2) and invoke a stress-strain equation to relate the stress to derivatives of the displacement (the strain ϵ). Since we are dealing with shocks of moderate strength we will allow for nonlinear elastic effects by going to second order in the strain as considered by Aboudi [20]

$$\sigma^{(\alpha,p)}(\overline{x},t)=E_\alpha\epsilon^{(\alpha,p)}(\overline{x},t)+\tfrac{1}{2}E'_\alpha[\epsilon^{(\alpha,p)}(\overline{x},t)]^2, \quad (2.2)$$

where E_α, E'_α are longitudinal elastic moduli (not to be confused with Young's modulus which applies to uniaxial stress conditions). The strain is derivative of the displacement with respect to the local cell position $\overline{x}$,

$$\epsilon^{(\alpha,p)}(\overline{x,t}) \equiv \frac{\partial u^{(\alpha,p)}(\overline{x,t})}{\partial \overline{x}} = \phi^{(\alpha,p)} + 3\overline{x}\,U^{(\alpha,p)}. \tag{2.3}$$

One then multiples Eq. (1.2) by $\overline{x^n}$ and integrates the resulting equation over subcell α. (As we shall see in Sec. II C, the full set of equations is derived by weighting the integrands with the various moments of $\overline{x}$ out to $n=2$.)

The solutions to these equations are subject either to external boundary conditions at the outer cells of the system $(\alpha=1,p=1)$ and $(\alpha=2,p=N)$

$$\sigma^{(1,1)}(-d_{1,1}/2,t)=\sigma_{app}(t), \tag{2.4}$$

$$\sigma^{(2,N)}(+d_{2,N}/2,t)=0, \tag{2.5}$$

for example, or to the conditions for displacement and stress continuity across each (internal) subcell interface. Between subcells $(1,p)$ and $(2,p)$ this condition demands

$$u^{(1,p)}(+d_{1,p}/2,t)=u^{(2,p)}(-d_{2,p}/2,t), \tag{2.6}$$

$$\sigma^{(1,p)}(+d_{1,p}/2,t)=\sigma^{(2,p)}(-d_{2,p}/2,t), \tag{2.7}$$

plus similar conditions at the interface of adjacent unit cells, $[(2,p)-(1,p+1)]$

$$u^{(2,p)}(+d_{2,p}/2,t)=u^{(1,p+1)}(-d_{1,p+1}/2,t), \tag{2.8}$$

$$\sigma^{(2,p)}(+d_{2,p}/2,t)=\sigma^{(1,p+1)}(-d_{1,p+1}/2,t). \tag{2.9}$$

For example, displacement continuity [Eqs. (2.6) and (2.8)] immediately yields two equations for the cell coefficients,

$$w^{(1,p)}+\frac{d_{1,p}}{2}\phi^{(1,p)}+\frac{d_{1,p}^2}{4}U^{(1,p)} = w^{(2,p)}-\frac{d_{2,p}}{2}\phi^{(2,p)}+\frac{d_{2,p}^2}{4}U^{(2,p)}, \tag{2.10}$$

and

$$w^{(1,p+1)}-\frac{d_{1,p+1}}{2}\phi^{(1,p+1)}+\frac{d_{1,p+1}^2}{4}U^{(1,p+1)} = w^{(2,p)}-\frac{d_{2,p}}{2}\phi^{(2,p)}+\frac{d_{2,p}^2}{4}U^{(2,p)}. \tag{2.11}$$

Here we adopt the shorthand notation of omitting the explicit time variable in $w^{(\alpha,p)}, \phi^{(\alpha,p)}$, and $U^{(\alpha,p)}$.

The result of carrying out this procedure is a set of equations that when combined with the stress continuity conditions, permit the entire set of cell coefficients $w^{(\alpha,p)}, \phi^{(\alpha,p)}, U^{(\alpha,p)}$, to be uniquely determined. We defer discussing these steps until Sec. II D. The present work deals with composites with one or more of its components being a polymeric material and hence it is first necessary to assume a slightly more generalized stress-strain relation. Including viscoelastic effects is our first extension of the Aboudi formalism, as we now discuss.

B. Viscoelastic effects

Certain classes of solid materials have physical properties resembling both those of elasticity and those of stress relaxation [8,22]. Compounds made up of large molecules, such as polymers, are examples. Under the action of an applied stress these materials do not deform instantaneously according to a simple time-independent stress-strain relation like Eq. (2.2). Rather, at a given time t and location, the stress generally depends on the deformation history. Also, these materials differ from viscoplastic solids in their ability to recover their shape when the applied stress is removed. A common way of handling these ''viscoelastic'' materials is by introducing a relaxation time τ_α into a *dynamic* elastic-stress-strain equation. If the application of stress is sufficiently fast the material will respond elastically in close accordance with Eq. (2.2), with (E_α, E'_α) being the relevant moduli. On the other hand, in the viscous domain at very low loading rates we expect the material will respond according to reduced or ''relaxed'' set of moduli (M_α, M'_α). The time scale for switching from one behavior to the other is controlled by τ_α and a scheme that interpolates from one type of behavior to the other is implemented by replacing Eq. (2.2) by the *standard viscoelastic-solid model* [8]

$$\dot{\sigma}^{(\alpha,p)}(\overline{x,t})-\dot{\epsilon}^{(\alpha,p)}(\overline{x,t})(E_\alpha+E'_\alpha\epsilon^{(\alpha,p)}(\overline{x,t})) = -\left(\frac{\sigma^{(\alpha,p)}(\overline{x,t})-M_\alpha\epsilon^{(\alpha,p)}(\overline{x,t})-\frac{1}{2}M'_\alpha[\epsilon^{(\alpha,p)}(\overline{x,t})]^2}{\tau_\alpha}\right). \tag{2.12}$$

Note again here that E_α, etc., are longitudinal elastic moduli corresponding to c_{11} in Voigt notation (not Young's modulus). The formal solution of this equation, which is consistent with the material being in a state of zero stress at $t=0$, is easily determined

$$\sigma^{(\alpha,p)}(\overline{x,t}) = \left(E_\alpha\delta_{t,t'}+\left[\frac{M_\alpha-E_\alpha}{\tau_\alpha}\right]\int_0^t dt' e^{(t'-t)/\tau_\alpha}\right)\times\epsilon^{(\alpha,p)}(\overline{x,t'})+\frac{1}{2}\left(E'_\alpha\delta_{t,t'}+\left[\frac{M'_\alpha-E'_\alpha}{\tau_\alpha}\right]\times\int_0^t dt' e^{(t'-t)/\tau_\alpha}\right)[\epsilon^{(\alpha,p)}(\overline{x,t'})]^2, \tag{2.13}$$

where each integral acts on the $\epsilon^{(\alpha,p)}(\overline{x,t})$ to the right of it.

To proceed further, the relaxed moduli (M_α, M'_α) can always be written in terms of the unrelaxed moduli as $E_\alpha=\nu_\alpha M_\alpha$ and $E'_\alpha=\nu'_\alpha M'_\alpha$. Without additional knowledge to the contrary we now make the simplifying assumption that $\nu_\alpha=\nu'_\alpha$, that is, the linear and nonlinear elastic moduli are reduced in the same proportion. This immediately allows Eq. (2.13) to be written succinctly as

$$\sigma^{(\alpha,p)}(\overline{x,t})=\mathcal{T}^{(\alpha,p)}(t)\{E_\alpha\epsilon^{(\alpha,p)}(\overline{x,t'})+\tfrac{1}{2}E'_\alpha[\epsilon^{(\alpha,p)}(\overline{x,t'})]^2\}, \tag{2.14}$$

where we have introduced a viscoelastic-relaxation *operator* $\mathcal{T}^{(\alpha,p)}(t)$, as

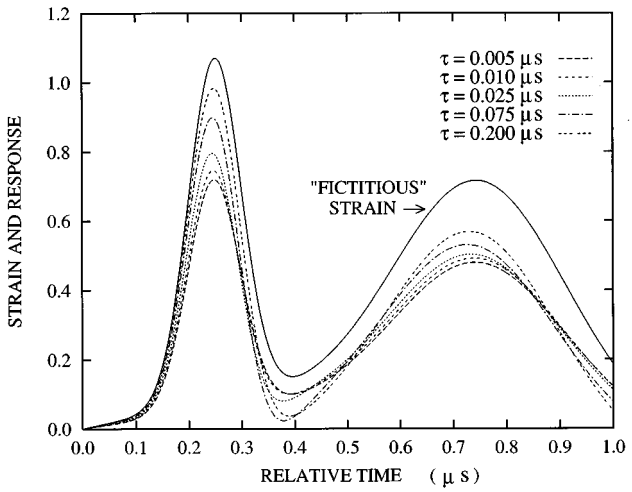

FIG. 2. Stress calculated from Eq. (2.19) for a ''fictitious'' input strain (solid curve) for various relaxation times τ. (The stress is in units of Mbar.)

$$\mathcal{T}^{(\alpha,p)}(t) \equiv \delta_{t,t'} + \left(\frac{\nu_\alpha - 1}{\tau_\alpha}\right) \int_0^t dt' e^{(t'-t)/\tau_\alpha} \quad ; \quad (2.15)$$

the integral acts on all time-dependent quantities to the right of it.

The strain from Eq. (2.3) can now be inserted into Eq. (2.14) to give the stress at any position $\overline{x}$, in cell (p,α) at any time once the cell coefficients, $w^{(\alpha,p)}, \phi^{(\alpha,p)}$, and $U^{(\alpha,p)}$, are known. Further, if the material is purely elastic the relaxation ratio $\nu_\alpha = 1$ and Eq. (2.14) still applies.

To give the reader a feel for the behavior of this relaxation function, a plot of a *fictitious* strain $\epsilon(t)$ and the stress calculated from the linear term in Eq. (2.14) is shown in Fig. 2 for various values of τ. The input strain field used in this figure is for illustration only and bares no direct connection to the numerical results of the following sections. The elastic modulus E is assigned a value of unity so that the stress exactly equals the strain when the relaxation contribution is zero. Thus any deviation in the stress curve from the strain reflects the importance of the relaxation function. The relaxation ratio ν was chosen to be 0.7. Two observations are notable. First, the longest relaxation times (the biggest τ) correspond most closely to an elastic solid — relaxation effects are smallest. Conversely, the shorter the relaxation time, the greater the stress tends to lag any change in the deformation. Second, short duration, large strain-rate processes are influenced less by the relaxation term.

C. Stress equations

We now return to integrating the equation of motion, as outlined in Sec. II A. Since the inclusion of viscoelastic effects produces only a minor complication to the Aboudi equations, via the introduction of the relaxation operator $\mathcal{T}^{(\alpha,p)}(t)$, we will maintain our attempt to keep the discussion brief.

Integrating the equation of motion over subcell α gives the zeroth moment equation,

$$\sigma^{(\alpha,p)}(+d_{\alpha,p}/2,t) - \sigma^{(\alpha,p)}(-d_{\alpha,p}/2,t) = \rho_{\alpha,p} d_{\alpha,p} \ddot{w}^{(\alpha,p)}. \quad (2.16)$$

Multiplying the equation of motion first by $\overline{x}$ and integrating gives the first-moment equation,

$$\sigma^{(\alpha,p)}(+d_{\alpha,p}/2,t) + \sigma^{(\alpha,p)}(-d_{\alpha,p}/2,t) - \frac{\rho_{\alpha,p} d_{\alpha,p}^2}{6} \ddot{\phi}^{(\alpha,p)} = \frac{2}{d_{\alpha,p}} \int_{-d_{\alpha,p}/2}^{+d_{\alpha,p}/2} \sigma^{(\alpha,p)}(\overline{x},t)\, d\overline{x}, \quad (2.17)$$

and similarly, multiplying by $\overline{x^2}$ and integrating produces the second-moment equation,

$$\frac{\rho_{\alpha,p}}{3} \ddot{w}^{(\alpha,p)} - \frac{d_{\alpha,p}^2 \rho_{\alpha,p}}{60} \ddot{U}^{(\alpha,p)} = \frac{1}{d_{\alpha,p}} \left(\frac{2}{d_{\alpha,p}}\right)^2 \times \int_{-d_{\alpha,p}/2}^{+d_{\alpha,p}/2} \sigma^{(\alpha,p)}(\overline{x},t)\, \overline{x}\, d\overline{x}. \quad (2.18)$$

It is a straightforward task to evaluate these integrals upon inserting the stress-strain equation [Eq. (2.14)]. Thereafter, Eqs. (2.16) and (2.17) can be added and subtracted to yield the stress evaluated at the (sub)cell interface

$$\rho_{\alpha,p} d_{\alpha,p} \left\{ \frac{d_{\alpha,p}}{6} \ddot{\phi}^{(\alpha,p)} + \ddot{w}^{(\alpha,p)} \right\} + 2\mathcal{T}^{(\alpha,p)}(t) \phi^{(\alpha,p)} = 2\sigma^{(\alpha,p)}(+d_{\alpha,p}/2,t) \quad (2.19)$$

and

$$\rho_{\alpha,p} d_{\alpha,p} \left\{ \frac{d_{\alpha,p}}{6} \ddot{\phi}^{(\alpha,p)} - \ddot{w}^{(\alpha,p)} \right\} + 2\mathcal{T}^{(\alpha,p)}(t) \phi^{(\alpha,p)} = 2\sigma^{(\alpha,p)}(-d_{\alpha,p}/2,t). \quad (2.20)$$

Inserting these into the stress continuity condition [Eq. (2.7)] for two adjoining subcells $[(1,p)-(2,p)]$ yields

$$\frac{\rho_{1,p} d_{1,p}}{2} \left\{ \frac{d_{1,p}}{6} \ddot{\phi}^{(1,p)} + \ddot{w}^{(1,p)} \right\} - \frac{\rho_{2,p} d_{2,p}}{2} \left\{ \frac{d_{2,p}}{6} \ddot{\phi}^{(2,p)} - \ddot{w}^{(2,p)} \right\} = \mathcal{T}^{(2,p)}(t) \phi^{(2,p)} - \mathcal{T}^{(1,p)}(t) \phi^{(1,p)}, \quad (2.21)$$

and two adjacent unit cells [Eq. (2.9) $(2,p-1)-(1,p)$]

$$\frac{\rho_{2,p-1} d_{2,p-1}}{2} \left\{ \frac{d_{2,p-1}}{6} \ddot{\phi}^{(2,p-1)} + \ddot{w}^{(2,p-1)} \right\} - \frac{\rho_{1,p} d_{1,p}}{2} \left\{ \frac{d_{1,p}}{6} \ddot{\phi}^{(1,p)} - \ddot{w}^{(1,p)} \right\} = \mathcal{T}^{(1,p)}(t) \phi^{(1,p)} - \mathcal{T}^{(2,p-1)}(t) \phi^{(2,p-1)}. \quad (2.22)$$

This gives two more (second-order integral-differential) equations for the cell coefficients. A third equation follows immediately by evaluating the integral in the second-moment equation, Eq. (2.18). The result is

$$\frac{\rho_{\alpha,p}}{3} \ddot{w}^{(\alpha,p)} - \frac{d_{\alpha,p}^2 \rho_{\alpha,p}}{60} \ddot{U}^{(\alpha,p)} = \mathcal{T}^{(\alpha,p)}(t) U^{(\alpha,p)}. \quad (2.23)$$

D. Method of solution

Equations (2.10), (2.11), (2.21), (2.22), and (2.23), along with the appropriate boundary conditions for the external

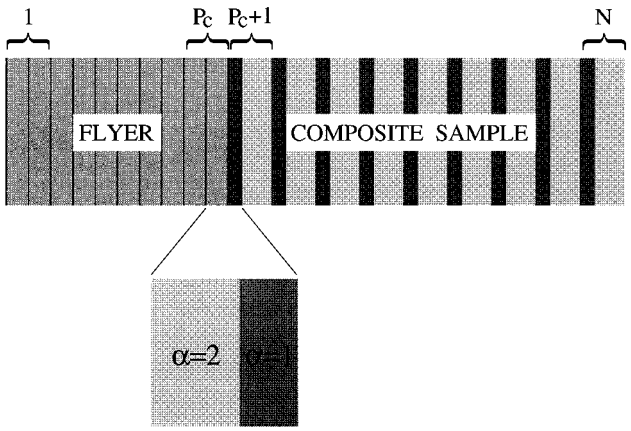

FIG. 3. Schematic of composite impact plate experiment. The homogeneous flyer material is also divided into cells for computation purposes. The impact interface is between subcells $(2,p_c)$ and $(1,p_c+1)$.

cells, provide a sufficient number of equations, to give a unique solution of the cell coefficients. Aboudi [20] has provided a useful algorithm for solving these equations, which for completeness we now outline. For each cell, there are six independent equations. The structure of these equations is such that they couple a given subcell with its two adjacent neighbors. (One subcell belongs to a neighboring unit cell, and one is the partner subcell to its own unit cell.) One can map, starting with $p=1$ cell, occupying the first six rows, the $p=2$ cell, occupying the next six rows, and so on, up to unit cell $p=N$, the entire set of equations onto a matrix equation of the form

$$\mathbf{A}\ddot{\mathbf{Q}}(\mathbf{t})=\mathbf{R}(\mathbf{t}), \tag{2.24}$$

where we have followed the notation of Ref. [20]. The matrix $\mathbf{A}$ is a $6N\times 6N$ parameter matrix constructed from the $d_{\alpha,p}$ and $\rho_{\alpha,p}$. The column matrix $\ddot{Q}(t)$ is composed of second-time derivatives of the cell coefficients

$$\ddot{Q}(t)=\begin{pmatrix} \ddot{w}^{(1,1)}(t) \\ \ddot{w}^{(2,1)}(t) \\ \ddot{\phi}^{(1,1)}(t) \\ \ddot{\phi}^{(2,1)}(t) \\ \ddot{U}^{(1,1)}(t) \\ \ddot{U}^{(2,1)}(t) \\ \vdots \\ \ddot{U}^{(2,N)}(t) \end{pmatrix} \tag{2.25}$$

and column matrix $R(t)$ consists of all terms in these equations containing no time derivatives. They include terms with the viscoelastic relation operator $\mathcal{T}^{(\alpha,p)}(t)$. Upon inverting $\mathbf{A}$ and representing the second-time derivative as a finite difference, the solution of the entire set of differential equations is gotten by the time evolution of

$$Q(t+\Delta t)=(\Delta t)^2\mathbf{A}^{-1}R(t)+2Q(t)-Q(t-\Delta t)\ . \tag{2.26}$$

We now determine the appropriate boundary conditions to simulate an impact experiment. These will provide the cell coefficients necessary to initiate the step-through solution of Eq. (2.26).

E. Flyer-target impact

Rather than introducing a stress wave into the system with $\sigma_{app}(t)$, as was done by Aboudi [11,20], in this section we derive the initial and boundary conditions consistent with the experimental setup of a flyer plate colliding with a stationary target. This is a standard experimental method for achieving large transient stress fields in a material. The flyer and target are not necessarily made of the same substance and the flyer can also be made up of sections of different materials. For example, in the experiment discussed below, the flyer plate consisted of a small slab of Z-cut quartz at the impact end, backed with a substantially larger slab of polymethylmethacrylate (PMMA). The PMMA is used to dampen the high frequency *ringing* in the flyer upon acceleration and before impact, and the entire system after impact. Consequently, it acts to stabilize the experiment. In fact, all internal transient motion in the flyer plate, arising when the flyer is set into motion, is assumed to have ceased by the time of impact —the flyer is assumed to be in a state of equilibrium. We assume that the sample sections remain intact, and the flyer and sample remain in contact throughout the measuring time for the experiment. These conditions are met in the experiment.

For discussion, we consider the reference frame where, before impact, the flyer plate approaches the target with a uniform velocity v_o and the target sample is at rest. To initiate the step-through procedure outlined in the preceding section, we seek values for the cell coefficients, $\{w^{(\alpha,p)},\phi^{(\alpha,p)},U^{(\alpha,p)}\}$, at $t=0$ and at $t=\Delta t$, i.e., at impact and one time step after impact.

To incorporate the flyer plate into the Aboudi formalism we first divide the homogeneous material(s) making up the flyer into (fictitious) unit cells (and each of these into two subcells for easy coding). Figure 3 shows a schematic of the setup. Let p_c denote the impact unit cell of the flyer; then cell p_c+1 is the first unit cell of the composite target. The impact subcell within cell p_c is the $\alpha=2$ subcell. Likewise the impact subcell of the target cell is the $\alpha=1$ subcell. Thus cells $\{1,2,\ldots,p_c\}$ refer to the flyer plate and cells $\{p_c+1,p_c+2,\ldots,N\}$ refer to the target. [Parenthetically, a window plate, attached to the target for detection is often also part of the system (see Sec. III A)].

We define $t=0$ to be the time just at the instant of impact — the cells are in contact but no compression of the cells has yet occurred. At that time, the unit cells $\{1,2,\ldots,p_c\}$ are all moving with uniform velocity v_o, and unit cells in the target, $\{p_c+1,p_c+2,\cdots,N\}$ are at rest. The relative displacements and the stresses between each unit cell and between each subcell are zero. Next, we can always choose Δt (the arguments for estimating an upper bound on Δt are unambiguous and are given below) small enough such that at time Δt, the subcells $(2,p_c)$ and $(1,p_c+1)$ are now in a state of

compression, all others are not. Subcells $\{(1,1),(2,1),(1,2),(2,2),\ldots,(2,p_c-1),(1,p_c)\}$ remain moving with uniform velocity v_o, and target subcells, $\{(2,p_c+1),(1,p_c+2),\ldots,(2,N)\}$ are still at rest.

These conditions are sufficient to determine cell coefficients at $t=0$ and Δt. Continuity of stress and displacement are forced at the impact interface $[(2,p_c)-(1,p_c+1)]$. At $t=\Delta t$ this translates into the two equations,

$$\sigma=\rho_{2,p_c}U_{2,p_c}\dot{u}_{2,p_c}=\rho_{1,p_c+1}U_{1,p_c+1}\dot{u}_{1,p_c+1} \tag{2.27}$$

and

$$(v_o-\dot{u}_{2,p_c})\Delta t=\dot{u}_{1,p_c+1}\Delta t\ , \tag{2.28}$$

where $\dot{u}_{\alpha,p}$ and $U_{\alpha,p}$ are the particle and shock speeds, respectively. Since the strain under these conditions is $\epsilon^{(\alpha,p)}=\dot{u}_{\alpha,p}/U_{\alpha,p}$ [10], we arrive at three equations for the three unknowns $\epsilon^{(2,p_c)}$, $\epsilon^{(1,p_c+1)}$, and u_{2,p_c}.

$$\begin{aligned}
&E_1+\tfrac{1}{2}E_1'\epsilon^{(1,p_c+1)}(\overline{x,t})=E_2+\tfrac{1}{2}E_2'\epsilon^{(2,p_c)}(\overline{x,t}),\\
&\rho_{1,p_c+1}(v_o-\dot{u}_{2,p_c})^2=[E_1+\tfrac{1}{2}E_1'\epsilon^{(1,p_c+1)}(\overline{x,t})]\\
&\qquad\qquad\times[\epsilon^{(1,p_c+1)}(\overline{x,t})]^2,\\
&\rho_{2,p_c}\dot{u}_{2,p_c}^2=[E_2+\tfrac{1}{2}E_2'\epsilon^{(2,p_c)}(\overline{x,t})][\epsilon^{(2,p_c)}(\overline{x,t})]^2,
\end{aligned} \tag{2.29}$$

where $\mathcal{T}^{(\alpha,p)}(t)\to 1$ is applicable. Only the values of $\dot{u}_{2,p_c}$ (and $\dot{u}_{1,p_c+1}$) are needed. Though it is not necessary to do so, rather than solving Eqs. (2.29) self-consistently, an analytic solution of $\dot{u}_{2,p_c}$ is possible if cubic strain terms are dropped; this step is easily justified and was done to avoid unnecessarily complicating the numerical work.

Continuity of the displacement at the impact interface yields the following constraint on the cell coefficients:

$$w^{(2,p_c)}+\frac{d_{2,p_c}}{2}\phi^{(2,p_c)}+\frac{d_{2,p_c}^2}{4}U^{(2,p_c)}=\dot{u}_{1,p_c+1}\Delta t,$$

$$w^{(1,p_c+1)}-\frac{d_{1,p_c+1}}{2}\phi^{(1,p_c+1)}+\frac{d_{1,p_c+1}^2}{4}U^{(1,p_c+1)}=\dot{u}_{1,p_c+1}\Delta t\ . \tag{2.30}$$

Similarly, the displacement and stress continuity at interfaces $[(1,p_c)-(2,p_c)]$ and $[(1,p_c+1)-(2,p_c+1)]$ give four more equations:

$$\begin{aligned}
&w^{(2,p_c)}-\frac{d_{2,p_c}}{2}\phi^{(2,p_c)}+\frac{d_{2,p_c}^2}{4}U^{(2,p_c)}=v_o\Delta t,\\
&w^{(1,p_c+1)}+\frac{d_{1,p_c+1}}{2}\phi^{(1,p_c+1)}+\frac{d_{1,p_c+1}^2}{4}U^{(1,p_c+1)}=0,\\
&\phi^{(2,p_c)}-\frac{3d_{2,p_c}}{2}U^{(2,p_c)}=0,\\
&\phi^{(1,p_c+1)}+\frac{3d_{1,p_c+1}}{2}U^{(1,p_c+1)}=0.
\end{aligned} \tag{2.31}$$

The solution of Eqs. (2.30) and (2.31), with $\dot{u}_{1,p_c+1}$ determined from Eq. (2.29), provide the desired $t=\Delta t$ boundary conditions

$$\begin{aligned}
&w^{(1,p_c+1)}=\tfrac{1}{3}\dot{u}_{1,p_c+1}\Delta t,\\
&\phi^{(1,p_c+1)}=-\frac{\dot{u}_{1,p_c+1}}{d_{1,p_c+1}}\Delta t,\\
&U^{(1,p_c+1)}=\frac{2}{3}\frac{\dot{u}_{1,p_c+1}}{d_{1,p_c+1}^2}\Delta t,\\
&w^{(2,p_c)}=\frac{\dot{u}_{1,p_c+1}}{3}(2v_o+\dot{u}_{1,p_c+1})\Delta t,\\
&\phi^{(2,p_c)}=\frac{1}{d_{2,p_c}}(\dot{u}_{1,p_c+1}-v_o)\Delta t,\\
&U^{(2,p_c)}=\frac{2}{3d_{2,p_c}^2}(\dot{u}_{1,p_c+1}-v_o)\Delta t.
\end{aligned} \tag{2.32}$$

Finally, a few words on estimating Δt are in order. Neglecting all considerations besides the impact itself that could require further restrictions on the choice of Δt, one can choose Δt to be some fraction of the lesser of $\Delta x_{2,p_c}/c_L^{(2,p_c)}$ and $\Delta x_{1,p_c+1}/c_L^{(1,p_c+1)}$. Here, $\Delta x_{\alpha,p}$ are the widths of the spatial grid for the two subcells nearest the impact interface. [Note that even the composite subcells can be zoned on finer mesh than the actual material subcell if necessary (see Sec. III A)]. Similarly, $c_L^{(\alpha,p)}$ are the corresponding longitudinal sound speeds. Since $c_L^{(\alpha,p)}=\sqrt{E_\alpha/\rho_{\alpha,p}}$, Δt can be estimated entirely in terms of the material properties. Taking one tenth of the smaller of the two numbers gives a reliable Δt.

III. NUMERICAL RESULTS

In this section we compare the generalized MOC results to data from the flat-plate impact experiment. Our goal is twofold. First, this comparison provides a rather stringent test of the theory. We find that because of the complexity of the setup (a large number of materials, etc.) estimates of

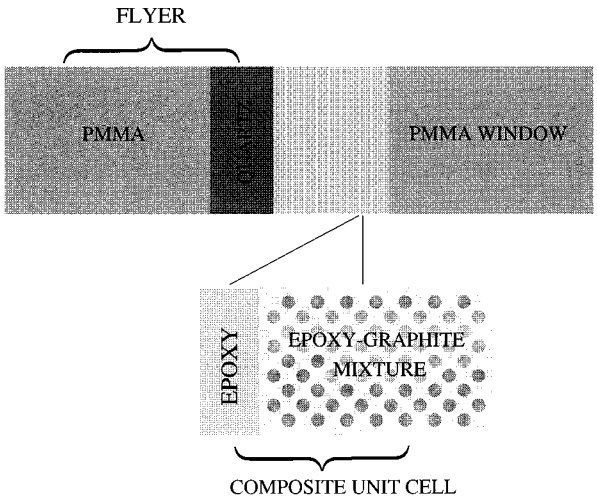

FIG. 4. Schematic of the experiment. The flyer consisted of a *Z*-cut quartz impactor, backed by a larger plate of PMMA. The composite was made of epoxy, epoxy graphite unit cells. The particle velocity at the composite-PMMA-window interface was measured by laser interferometry.

many material properties are necessary. This includes not only the viscoelastic τ and ν for the polymeric compounds, but also the nonlinear elastic moduli E' for all the materials. We emphasize that it is *not* our goal to do an extensive search over a large-as-feasible parameter space, but rather to use whatever data we have on these materials to deduce reasonable estimates for the parameters. We believe this provides a more honest representation of versatility of the method, albeit probably not the best fit to the experimental data but one that emphasizes the importance of having adequate material property data independent of the experiment being analyzed.

Second, we hope to shed light on some of the salient features of the experimental results that have not yet been explained by other theoretical methods. In our first set of calculations we assume that the composite has translation symmetry in its cell structure. This hypothesis is tested in Sec. III E by allowing subcell widths in the composite to vary randomly. In fact, this example has more than pedagogic importance because the composite in the experiment has a visible amount of irregularity in its cell widths.

A. Experimental measurement

A schematic of the flyer, composite sample, and window for the experiment is shown in Fig. 4; the dimensions and mass densities for these are given in Table I. The flyer plate in this experiment was *Z*-cut quartz, backed by PMMA and inserted into an aluminum projectile. Quartz in this orientation was chosen for its high Hugoniot elastic limit (HEL). The projectile was accelerated using a single stage 72 mm bore gas gun facility, achieving a velocity of 0.5003 km/s. Projectile tilt was not measured in this experiment, but from previous measurements is assumed to be less than 2 mrad. This implies a very planar impact which means the composite target was subjected to uniaxial strain. The composite target was oriented with laminations normal to the impact direction, was backed by a PMMA window, and had a thin (0.025 mm) aluminum foil between the target and window to provide a reflective surface. This reflective surface allowed time-resolved particle velocity information to be measured using a VISAR (velocity interferometer system for any reflector) velocity interferometer [23]. The VISAR system used for the experiment was configured with a relatively long delay leg to yield high particle velocity resolution. Particle velocity was measured at the target-window interface yielding an approximate *in situ* measurement.

TABLE I. Flyer, sample, and window dimensions and densities in the composite experiment.

Component	Length (mm)	ρ (g/cm^3)
	Flyer	
PMMA[a]	5.000	1.15
Z-cut quartz	1.557	2.65
	Composite[b]	
Epoxy subcell	0.027	1.270
Epoxy-graphite subcell	0.120	1.630
	Window	
PMMA	5.000	1.15

[a]PMMA is the standard abbreviation for polymethylmethacrylate
[b]The composite consisted of 19 unit cells making up a total length of 2.806 mm.

The composite portion of the system consisted of 19 nearly equal-width unit cells, each containing two subcells. One subcell consisted of an epoxy-graphite mixture, and the second, much thiner subcell was made of pure epoxy. We refer to the epoxy-graphite subcell as 1, and the pure epoxy subcell as 2. Approximately 39% of the volume of subcell 1 was graphite and the remaining volume was filled with epoxy. The graphite was shaped into unidirectional fibers oriented parallel to neighboring subcell walls and distributed uniformly throughout the subcell.

B. Elasto-mechanical properties

To apply the MOC to this system requires substantial knowledge of the elastic and viscoelastic properties of the materials comprising the system. For a material like PMMA much is known from previous high-quality experiments. [24] Unlike for many homogeneous materials, however, the elastic properties of the epoxy-graphite mixture are not previously tabulated. Nevertheless, sufficient information was measured on the experimental system to deduce these.

The longitudinal sound velocity and the average density were both measured for the entire composite: $\overline{c_L}=2.855$ mm/μs and $\overline{\rho}=1.564$ g/cm^3. The longitudinal sound velocity for pure epoxy, its mass density, and the mass density of pure graphite are all known [25] or measured independently here: $c_L^{(2)}=2.520$ mm/s, $\rho_2=1.27$ g/cm^3, and $\rho_{\text{graphite}}=2.20$ g/cm^3, respectively. Finally, the average subcell widths d_1 and d_2, were extracted from an optical metallograph of the composite ($d_1=0.120$ mm, $d_2=0.027$ mm). With this information in hand, we can estimate the elastic moduli of subcell 2 and the average moduli for the entire composite. We find, $E_2=\rho_2[c_L^{(2)}]^2$

TABLE II. Flyer, sample, and window elastic moduli, relaxed moduli, and relaxation times for the composite experiment.

Component	E (g cm/μs^2)	E' (g cm/μs^2)	ν	τ (μs)
		Flyer		
PMMA	0.089	−0.72	0.75	0.01
Z-cut quartz	1.072	−5.83	1.0	
		Composite		
Epoxy subcell	0.186	−0.93[a]	0.90	0.015
Epoxy-graphite subcell	0.146	−0.88	0.88	0.025
		Window		
PMMA	0.089	−0.72	0.75	0.01

[a]See comment on epoxy in Sec. III D.

$=0.081$ Mbar, and $\overline{E}=\overline{\rho c_L^2}=0.127$ Mbar. (Note that 1 Mbar = g cm/μs^2). Next we seek ρ_1, the effective mass density of the epoxy-graphite component. To that end, we note that the volume fraction for subcell 1 relative to the *full* unit cell is $\phi_1=d_1/(d_1+d_2)$. Since

$$\overline{\rho}=\rho_2(1-\phi_1)+\rho_1\phi_1 \tag{3.1}$$

we find immediately that $\rho_1=1.630$ g/cm^3. Similarly, since the average modulus for the composite is related to its constituent moduli by

$$\frac{1}{\overline{E}}=(1-\phi_1)\frac{1}{E_2}+\phi_1\frac{1}{E_1}, \tag{3.2}$$

we can solve for the elastic moduli for the epoxy-graphite subcell. The result is $E_1=0.146$ Mbar. This gives a sound speed of 0.299 cm/μs for that material.

The nonlinear elastic moduli E', have to be estimated for the PMMA, quartz, epoxy, and epoxy-graphite mixture. This can be done as follows. It is well documented [10,26] that the shock speed (U_s) varies linearly with the particle speed (U_p)over a substantial range; the relation is $U_s=c+sU_p$, where c is the zero pressure bulk sound velocity [27] and s is the slope. Material porosity, elastic-plastic transition, and phase transitions are the usual causes of departure from linearity. For the materials of interest to us here, U_s, U_p measurements have been done elsewhere and their s are tabulated [25]. We can use our knowledge of s to arrive at an estimate for E' since $\sigma=\rho U_p U_s$ and $\epsilon=U_p/U_s$ imply that

$$\sigma=\rho U_s U_p=\rho(c_L+sU_p)U_p=(\rho c_L^2)\epsilon+(2\rho c_L^2 s)\epsilon^2+\cdots. \tag{3.3}$$

Comparing with the static-stress-strain equation (Eq. 2.2) allows us to identify E with ρc_L^2 and E' with $4Es$. (In our numerical work we apply the convention that stresses are negative in compression and thus, $E'=-4Es$, is used.)

The mass density and elastic modulus E are well known for PMMA. To obtain values for E', ν, and τ we look to the work of Schuler and Nunziato [24] whom have investigated the elasto-mechanical properties of PMMA in considerable detail. Using a plate impact experiment, they measured the shock speed as a function of the particle speed, from which we can estimate the slope s. From their data we extract a value of s approximately equal to 2, pertaining to stress that the PMMA is subjected to in the experiment. From our estimate $E'=-4Es$, we then arrive at $E'=-0.72$ Mbar. Schuler and Nunziato also provide a means of estimating the relaxation time. They found that their data fit well a stress-dependent relaxation function of the form,

$$\tau=\tau_o\exp\left[-\left(\frac{\sigma-\sigma_E}{k}\right)\right], \tag{3.4}$$

where $\tau_o=0.25$ μs and $k=0.8$ kbar are constant parameters fitted to the data. Here, σ_E is the equilibrium stress, i.e., the stress state to which the material relaxes at constant strain, when the strain is held fixed for all time, and σ is the instantaneous stress. At 17 kbar one can extract from their measurements, values of $\sigma-\sigma_E$ in the range 2 kbar$\leqslant\sigma-\sigma_E\leqslant$4 kbar, giving a rather wide range of possible relaxation times of 0.002 μs$\leqslant\tau\leqslant$0.02 μs. Their data are consistent with a relaxation ratio of $\nu\approx0.75$.

The tabulated values [25] of s for pure epoxy and quartz are 1.543 and 1.36, respectively, giving values of $E_2'=-0.50$ Mbar and $E'_{\text{quartz}}=-5.83$ Mbar. For the epoxy graphite mixture we estimate $s=1.5$, which follows simply because this value is common to many materials. The relaxation times τ for the epoxy is not expected to deviate substantially from those of the PMMA. The elastic moduli in Table II were obtained in this manner.

Finally, we mention our layout (zoning) of the subcell widths used in our numerical work. The entire system was divided into 158 subcells. Rather surprisingly, the quartz impactor did not require fine zoning; it was found to be sufficient to divide the entire plate into 10 equal-width subcells with $d_1=d_2=0.015\,57$ cm. On the other hand, the composite required more careful consideration. With nonlinear elasticity included [the second term in Eq. (2.2)] *unphysical* oscillations were found to be a common problem in the numerical solutions. This could be eliminated somewhat by making the composite subcells to be approximately equal width. To do this we further divided the epoxy graphite subcells into three equal-width (sub)subcells, each with width 0.004 cm. After this, each unit cell had three identical neighboring graphite-epoxy subcells and one $d_2=0.0027$ cm epoxy subcell. Altogether the composite consumed 78 computational subcells. Finally, it was found that the impact side of

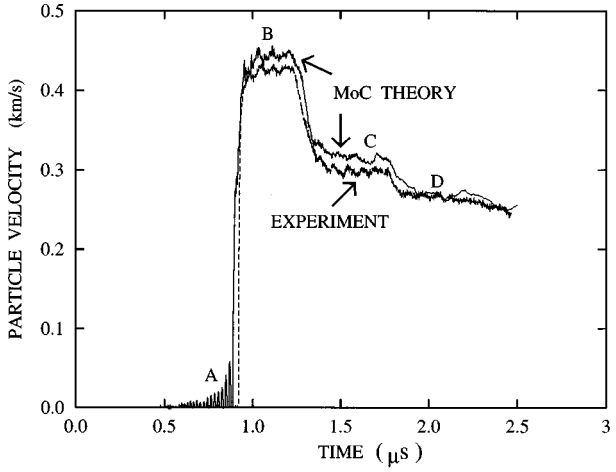

FIG. 5. Experimental and theoretical velocity profiles for waves propagating in the system shown in the preceding figure. Measurements are taken at the composite-window interface. The oscillations at (A) are unphysical. The particle velocity plateau at (B) is from the initial loading wave. The velocity at (C), and then again at (D), results when release waves arrive at the window.

the PMMA window also required very fine zoning. This was accomplished by dividing the forward segment of the window into 50 equal-width subcells, each having width of 0.0025 cm. The remaining window and the PMMA portion of the flyer required only a coarse grid. The reason for the small subcell widths in the window, near the impact surface, was to be certain that our numerical solution would be sensitive to all incoming deviations in the stress and velocity, including the very high frequency *ringing* that arises from reflections within the smallest subcells of the composite (in our case, this was the epoxy subcells).

C. Comparison of theory and experiment

In Fig. 5 the experimental and theoretical particle velocity profiles (velocity as a function of time) are shown. The origin of the time axis is placed at the instant of impact determined by the theory. Since absolute times were not recorded in the experiment, we have taken the liberty of positioning the experimental curve to match the theoretical one at the steepest rise in the velocity, i.e., at the acceleration maximum. In the theory, the particle velocity is simply the time derivative of the MOC displacement given by Eq. (2.1). In both the experiment and the theory, measurements were recorded at the composite-window interface. We begin by first giving a rather ''generic'' explanation of the physics behind the profile as seen by the detector located at the composite-window interface.

About 0.9 μs after impact the velocity wave reaches the observation point. Within a very short (but finite) duration, the particle velocity goes from zero to a value of approximately 0.42 km/s. This peak in the profile (labeled B in the figure) is caused by the main compression wave of the shock reaching the observation point. For obvious reasons this wave is commonly referred to as the loading wave. The physical region in front of the shock wave is still uncompressed, but behind the shock the system is in a state of compression. At about 0.3 μs after the arrival of the loading wave, there is a rather abrupt drop in the particle velocity, indicating that a release wave has arrived at the observation point. Its origin is the following. At impact, stress continuity tells us that a backward propagating compression wave in the Z-cut quartz impactor must accompany the forward propagating wave in the composite. The strength of the compression waves are equal at impact, and their respective speeds are given by the solution of Eqs. (2.29). The backward propagating compression wave will travel unimpeded in the flyer until it reaches the quartz-PMMA interface at which time a portion is transmitted into the PMMA and a portion is reflected back towards the window.

Because of the long length of the PMMA, and its lower sound speed, the portion transmitted into the PMMA will have detectable consequences only at times much larger than the measuring times in the experiment (and theory). Consequently, from here on we will only follow the reflected portion of the wave. Since the backward propagating compression wave is traveling in a higher acoustic impedance material (quartz) and is partially reflected from the interface of a lower impedance material (PMMA) the reflected wave will be a release wave, i.e., a rarefaction wave (note, acoustic impedance $\equiv\sqrt{\rho E}$). Also, only a portion of the backward moving compression wave is reflected, so the magnitude of the rarefaction is only a fraction of the initial compression. As the reflected wave strikes the quartz-composite interface, again transmission and reflection takes place. Ignoring, for the moment, the structure of the composite, the component transmitted into the composite acts to release some of the stress built up from the initial the loading wave. The final important fact is that waves propagating in the compressed region behind the shock front will propagate faster (supersonically) than in the uncompressed material. Consequently, the *release* wave catches up slightly and reaches the observation point about 1.3 μs after the initial impact.

In the figure the initial loading wave elevates the particle velocity to 0.42 km/s. The particle velocity stays at that value (the flyer continues to push the target) until the release wave arrives, thus reducing the particle velocity to 0.3 km/s. Yet, one more major reverberation occurs in the experiment 1.8 μs after impact. At that time a second release wave, after traversing the quartz twice, arrives at the observation point. Again, this wave reduces the stress and the particle velocity (down to point C in the figure) but by a correspondingly smaller amount.

Overall, the agreement between the MOC theory and the experiment is quite satisfactory. For the material parameters chosen, the MOC particle velocities tend to be slightly higher than those of the experiment. These material parameters represent our best objective estimates from independent measurements. We reemphasize that our goal was not to do an *ad hoc* adjustment of the material parameters until achieving a suitable fit. (In fact, increasing E_{PMMA} from 0.09 Mbar to 0.10 Mbar is all that is needed to make the MOC plateaus agree with the experimental ones.) In Sec. III D we comment on the small but well-defined oscillations visible in this figure. Not surprisingly, the MOC calculation reveals that these oscillations are a manifestation of the composite structure. Further, nonlinear elasticity plays an important role in achieving a quantitative description of this fine-detailed structure, and will also be discussed.

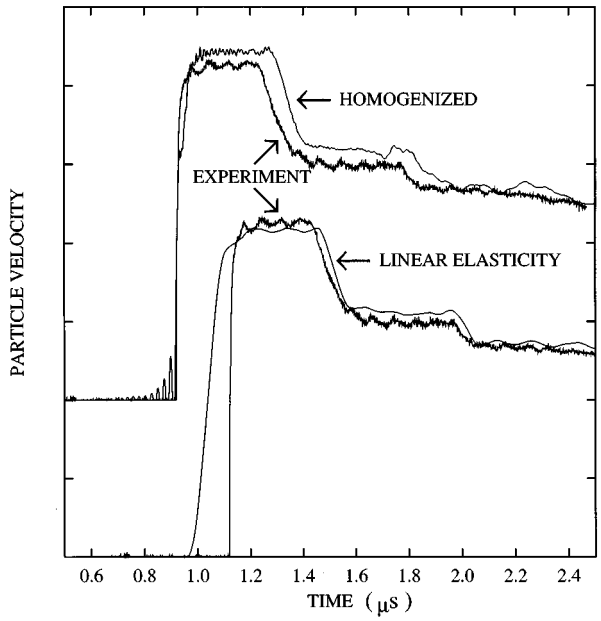

FIG. 6. Theoretical velocity profiles arrived at by omitting nonlinear elastic contributions (bottom profile) and by replacing the discrete cell structure of the composite by a continuum (top profile). The experimental profile is also shown.

D. Nonlinear elasticity and homogenization

As explained in preceding sections, nonlinear elasticity is incorporated into the theory by keeping terms to second order in the strain in the stress-strain relation Eq. (2.14). By including this contribution one can assess both its attributes and its undesirable qualities. First, the nonlinear terms are responsible for *unphysical* high frequency oscillations in the stress and velocity waves (point A in Fig. 5) preceeding the main (physical) pulse. By increasing the modulus E' to larger and larger values, these oscillations can become visible in region B. (It was for this reason that we reduced our estimate of E' for the epoxy subcell by 20% of the $-4sE$ value.)

The fact that the oscillations are unphysical is self-evident — they propagate ahead of the shock wave. Further, while their intensity is linked slightly to complicated cell structures, these oscillations persist in an homogenized approximation for the composite (discussed momentarily). Regardless of this undesirable property we state unequivocally that obtaining results in quantitative agreement with experiment *require keeping the nonlinear elastic terms*. To illustrate this, we show in Fig. 6 a velocity profile obtained by keeping only linear terms. Even though the agreement is visibly poor (the rise time of the loading wave is too large and the physical oscillations are greatly reduced), an adjustment was still required to achieve this level of agreement; we replaced the nonlinear material (variable acoustic impedance) with an equivalent linear elastic material with a constant acoustic impedance corresponding to this level of compression. To make the experimental and theoretical plateau heights comparable, we increased E_{PMMA} from the known value of 0.09 Mbar to 0.138 Mbar. We obtained the latter value by using the experimental observation that upon loading, the particle velocity in the PMMA reaches a value of 0.42 km/s. By arguments similar to those in the derivation of Eq. (3.3) we can arrive at an expression for an average E that effectively includes effects of second-order terms

$$E_{eff}=(\sqrt{E}+sU_p\sqrt{\rho})^2\ , \tag{3.5}$$

which yields $E_{eff}\approx 0.138$ Mbar, upon inserting the material parameters.

In Fig. 6 we also illustrate the important role that the composite cells have in determining the low amplitude well-defined oscillations observed at points (B) and (C), and to a lesser degree at (D) in Fig. 5. We first homogenized the composite by replacing the material cells with a single material that has effectively the same average properties. Upon doing so we find that the small oscillations are largely removed. [The anomalous precursor oscillations (at A) and the very high frequency oscillations at (B), associated with the nonlinear elastic term, remain however.] The homogenization used the experimentally determined sound speed and average density for the entire composite (see Sec. III B): $\overline{c_L}=2.855$ cm/μs and $\overline{\rho}=1.564$ g/cm^3. Recall that these are consistent with $\overline{E}=0.127$ Mbar. As usual, it is difficult to estimate values for $\overline{\tau,\nu}$ and $\overline{E'}$. Since this calculation is only for demonstration, we simply used the epoxy values of the preceding section. The composite length remained as before. Previous calculations on this system based on the MOC have invoked homogenization from the start and find similar flat, structureless plateaus in the velocity profile. [18] The present calculation is the first one based on the MOC that keeps the full cell structure for this (and to our knowledge any other) plate impact problem.

E. Effects of disorder

We now examine the effect of adding a small amount of ''disorder'' to the composite. Obviously, one can do this in several ways. For example, the amount of graphite in a given composite subcell varies somewhat from cell to cell. The cell dependence of the mass density is sufficient to break the translational symmetry of the composite. In the experiment this is probably a small effect since the epoxy graphite mixture appears to be quite homogeneous. Another example, the one tested here, is to allow the cell *width* to vary from subcell to subcell. This was the case in the composite used in the experiment. The values of subcell widths d_1 and d_2 used in the preceding section, are estimates of the average subcell widths. In fact, it is difficult to determine quantitatively the amount of variation in the cell widths. Consequently, we hope to use the MOC to help answer this question.

A random component can be incorporated into the cell widths in several different ways. For our purposes we have chosen to keep each unit cell width, d_1+d_2, fixed at the value of 0.0147 cm used in previous sections. Within each unit cell, however, we will allow the subcell widths to vary from one unit cell to the next (with the above restriction). In our numerical work, this was done by adding a randomly chosen width increment to a minimum tolerable width. The result was then normalized to fix the unit cell width ($d_{1,p}+d_{2,p}=0.0147$ cm). By proceeding this way, any given subcell width could be kept from becoming measurably less than its neighbors, a circumstance that can compromise the

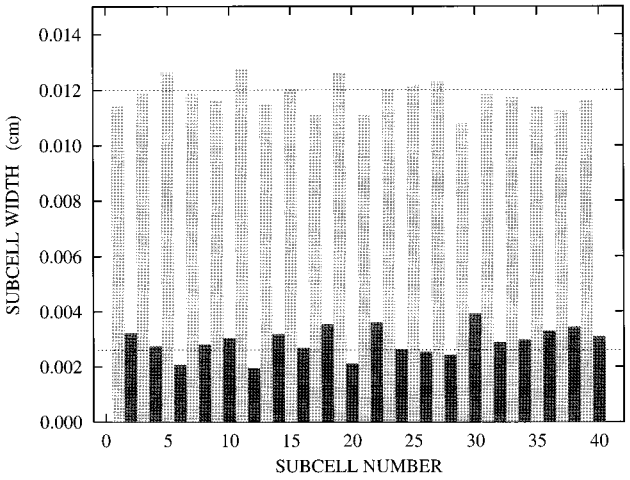

FIG. 7. Distribution of composite subcell widths, with a random component added. The horizontal dashed lines represent the subcell widths used in the periodic cell calculation. Although the individual subcell widths are random, the total width of each unit cell is fixed at the value used in the periodic case.

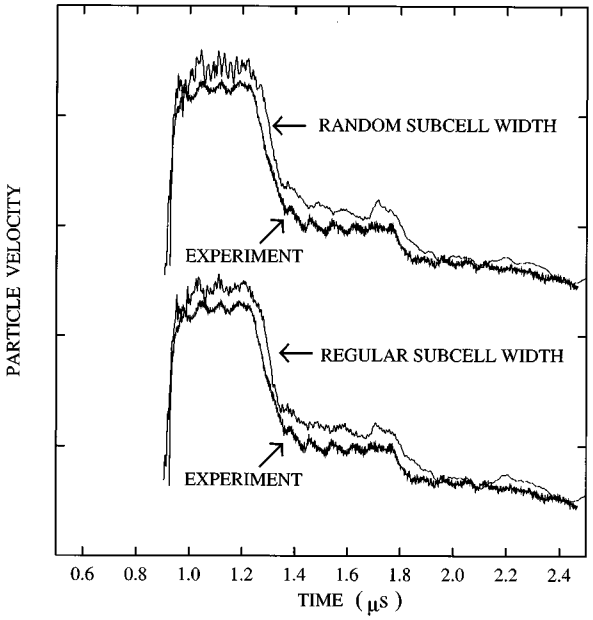

FIG. 8. Comparison of theoretical velocity profiles obtained with periodically repeating unit cells in the composite (bottom profile) and with the subcell width distribution shown in the preceding figure (top profile).

accuracy of the numerical solution. In Fig. 7, a representative cell width distribution is displayed. The longer (shorter) cell widths belong to the epoxy graphite (epoxy) subcells. The horizontal dashed lines indicate the average widths used in in the preceding sections for subcells 1 and 2.

The effects on the velocity profile from including disorder into the system can be seen from Fig. 8. For comparison, the experimental profile is also included. The theoretical periodic and disordered calculations used exactly the same set of elastic and relaxation parameters as input (those listed in Table II). It is clear from the figure that random subcell widths, to the amount given in Fig. 7, has several visible effects on the profile. The high frequency structure residing on the loading portion of the velocity profile (point B in Fig. 5) is considerably more chaotic and less well defined than in the periodic case. On the other hand, the oscillations in region C, after the arrival of the first release wave displays only small changes. This rather surprising result may be caused by the fact that the region behind the release wave is at a much lower pressure than behind initial loading wave. To test this hypothesis we lowered the impact velocity to a value of 0.3 km/s and observed the effects of disorder on the loading wave (point B). This result supports the hypothesis since the incorported disorder had noticably less effect than for the higher impact case. This demonstrates the complicated interplay between the cell structure, the nonlinear elasticity, and the wave propagation in this calculation. Finally, returning to the original question, our conclusions are that the composite used in the experiment has very little cell-width disorder since the small oscillations are well defined and clearly visible in the experimental data.

IV. SHORTCOMINGS OF THE MOC

From the results of the previous sections it is clear that the MOC is a useful and versatile tool for investigating transient propagation in rather complex materials. Even though this may be the case, we close the discussion with some critical comments regarding the MOC.

The first point we mention is obvious but important: The theory requires considerable input from material parameters, some of which are phenomenological parameters needed in the viscoelastic theory. The elastic modulus E can be obtained in principal, from adiabatic stress-strain measurements or adiabatic sound wave experiments, or from microscopic calculations and even computer simulations. To a lesser degree, this is also true for E'. On the other hand, only in a few exceptional cases (PMMA is an example) have studies been done to determine the relaxation parameters for viscoelastic materials in high stress fields. As a result, depending on the complexity of the setup and the materials, one can find themselves in a situation of having too many ''adjustable parameters'' to achieve trustworthy results. Certainly for the complicated setup in the experiment it is important to have independent, reliable experimental data at hand for the individual constituents.

Our second point concerns truncating the Legendre series for the displacement. To be confident of the quality of the the MOC expansion it would be desirable to carry out a calculation for $\mathcal{N}=1$, and then $\mathcal{N}=2$, and so on, until the numerical results are independent of the $\mathcal{N}$ used. In our work, we did this for $\mathcal{N}=1$ and 2. As a result, we found that the $\mathcal{N}=1$ expansion captured the magnitude of the stresses and velocities with surprising accuracy, but overall the results are more choppy than for $\mathcal{N}=2$ expansion. This is easily understood because the stress calculated at the level $\mathcal{N}=1$ is independent of the local variable $\bar{x}$; the stress within a subcell is a constant. Thus the stress, when plotted as a function of position has a histogramlike shape. Going to higher and higher order in the truncation gradually removes this defect. For example, at $\mathcal{N}=2$ the stress varies linearly with $\bar{x}$ allow-

ing for the possibility of more closely matching of slopes on the two sides of an interface.

Third, the MOC is entirely a mechanical theory. Without incorporating more formalism into the method we have precluded a proper treatment of the thermodynamics of dissipative processes [28], including nonadiabatic effects, and a proper treatment of plastic flow (which is important in composites made of metals with low yield strengths, e.g., copper and aluminum). Certainly this does not exhaust the list of possibilities.

V. CONCLUSIONS

In spite of the various qualifications we have raised to the application of the method of cells in real wave-propagation applications in composite materials, the method is really quite versatile. Here we included (1) sudden impact, (2) nonlinear elasticity, (3) viscoelasticity, and (4) arbitrary (nonperiodic) layering. The calculated results (for $\mathcal{N} = 2$) give a reasonably good representation of the actual experimental data in the case of a moderately simple, layered composite. Improvements in these calculations require comprehensive data on the component materials and perhaps extension of the theory to displacement expansions of orders higer than $\mathcal{N} = 2$. These are not easy problems to overcome in practical situations. Thus, when it appears necessary to include detailed effects of composite material behavior in applied wave-propagation situations, it would probably be prudent to examine the overall commitment and experimental resourses that can be brought to bear on the problem.

ACKNOWLEDGMENTS

The financial support of the Joint DoD/DoE Munitions Technology Development Program is appreciated. B.E.C. is grateful D. C. Wallace for discussions on shock waves, their thermal properties, and plastic flow. Discussions with F. L. Addessio and T. O. Williams regarding the method of cells are also gratefully acknowledged.

[1] L. Brillouin, *Wave Propagation in Periodic Structures* (McGraw-Hill, New York, 1946).
[2] J. C. Peck, in *Shock Waves and the Mechanical Properties of Solids*, edited by J. J. Burke and V. Weiss (Syracuse University Press, New York, 1971), Chap. 3, pp. 155–184.
[3] J. C. Peck and G. A. Gurtman, J. Appl. Mech. **36**, 479 (1969).
[4] J. Aboudi, *Mechanics of Composite Materials: A Unified Micromechanical Approach* (Elsevier, Amsterdam, 1991).
[5] J. Aboudi, Int. J. Eng. Sci. **19**, 1269 (1981).
[6] C. T. Sun, J. D. Achenbach, and G. Herrmann, J. Appl. Mech. **35**, 467 (1968).
[7] T. C. T. Ting and I. Mukunoki, J. Appl. Mech. **46**, 329 (1979).
[8] H. Kolsky, *Stress Waves in Solids* (Dover, New York, 1963).
[9] K. H. de Haas, G. J. Ruiter, and J. Mellema, Phys. Rev. E **52**, 1891 (1995).
[10] J. A. Zukas, T. Nicholas, H. F. Swift, L. B. Greszcuk, and D. R. Curran, *Impact Dynamics* (Krieger, Malabar, Florida, 1992).
[11] J. Aboudi, Wave Motion **9**, 141 (1987).
[12] V. Baluni and J. Willemsen, Phys. Rev. A **31**, 3358 (1985).
[13] J. P. Lu and J. L. Birman, Phys. Rev. B **38**, 8067 (1988).
[14] V. A. Hopkins, J. Keat, G. D. Meegan, T. Zhang, and J. D. Maynard, Phys. Rev. Lett **76**, 1102 (1996).
[15] M. L. Wilkins, in *Methods in Computational Physics*, edited by B. Alder, S. Fernbach, and M. Rotenberg (Academic, New York, 1964), Vol. 3, p. 211.
[16] J. N. Johnson, J. Appl. Phys. **52**, 2812 (1981).
[17] J. Aboudi, Int. J. Eng. Sci. **22**, 439 (1984).
[18] J. Aidun and F. Addessio, Los Alamos National Laboratory, Report LA12904-MS, 1995 (unpublished).
[19] J. Aboudi, Int. J. Engng Sci. **25**, 1229 (1987).
[20] J. Aboudi, in *Joint ASME/SES Applied Mechanics and Engineering Sciences Conference, Berkeley, California, June, 1988*, edited by A. K. Mal and T. C. T. Ting (AMD, New York, 1988), Vol. 90, p. 133.
[21] J. Aboudi, Wave Motion **8**, 289 (1986).
[22] Landau and Lifshitz, *Theory of Elasticity, A Course in Theoretical Physics* (Pergamon, Oxford, 1986), Vol. 7.
[23] W. F. Hemsing, Rev. Sci. Instrum. **50**, 73 (1989).
[24] K. W. Schuler and J. W. Nunziato, Rheol. Acta **13**, 265 (1974).
[25] *LASL Shock Hugoniot Data*, edited by S. Marsh (University of California Press, Berkeley, 1980), p. 446.
[26] R. G. McQueen *et al.*, in *High-Velocity Impact Phenonema*, edited by R. Kinslow (Academic, New York, 1964), Chap. 12, pp. 393–417.
[27] The more general relation is $c = \sqrt{c_L^2 - (4/3)c_s^2}$, for cases when the shear speed c_s is not zero.
[28] D. C. Wallace, Los Alamos National Laboratory, Report LA10119, 1985 (unpublished).